Spatiotemporal Electrochemistry on Flexible Microelectrode Arrays: Progress Towards Smart Contact Lens Integration

Contents lists available at ScienceDirect

Sensors & Actuators: B. Chemical

journal homepage: www.elsevier.com

Spatiotemporal electrochemistry on flexible microelectrode arrays: Progress towards smart contact lens integration

Matthew Donora *, Eva Gonzalez-Fernandez , Andrés Vásquez Quintero , Herbert De Smet , Ian Underwood

University of Edinburgh, United Kingdom

ARTICLE INFO

Keywords:
Flexible microelectrodes
Electrochemical methods
Wearable sensors
Smart contact lenses
Spatiotemporal electrochemistry

ABSTRACT

We demonstrate a real-speed spatiotemporal electrochemical map showing both time- and position-varying concentration of an analyte in contact with a flexible microelectrode array. A polymer-based device of 11 μm in thickness comprising patterned gold metallisation on a polyimide substrate was fabricated, with eight individually addressable working electrodes (diameter 30 μm) and an integrated counter electrode. We performed a repeated sequence of high-speed chronoamperometric measurements at each electrode and processed the data to generate a spatiotemporal concentration map, in which a number of fluid effects, including bulk flow, diffusive mixing and homogenisation of two miscible fluids of different concentration were observed. This device was fabricated using processes compatible with an existing smart contact lens platform, with a view to develop integrated sensors in future work. We believe this technique has significant potential in the field of electrochemical smart contact lenses, both in introducing new functionality and in improving our ability to draw accurate and clinically-relevant conclusions from measurements made in the tear film.

1. Introduction

Progress towards electrochemical sensing in smart contact lenses (SCLs) passed some significant milestones in the years following 2010 with, for example, the demonstration of the first electrochemical devices on a curved, flexible, transparent platform [1–4]; integration of wireless communication and power [5–8]; and the clinical use of a SCL containing a strain gauge sensor as a medical device [9,10]. Thus, the field of electrochemical smart contact lenses (ESCLs) may have appeared close to creating a viable product. However, progress may have slowed, with only a few public demonstrations in the second half of the decade [11,12]. In short, there is still work to be done on the integration of electrochemical sensors into unobtrusive wearable medical devices in general. Issues with materials used, such as polyethylene terephthalate (PET), and the ability to integrate sensors onto the curved surface of a soft contact lens platform [13] represent challenges which must be addressed before the transition from research into clinical practice.

Even less clearly understood are the advances necessary in the design of the electrochemical sensors for ESCLs. Initial efforts have often encountered a common problem, which is that the data obtained from an ESCL are not sufficiently correlated with the underlying concentration profile of the biomarker under analysis (usually the concentration in blood) to draw sufficiently accurate and robust conclusions relating to medical diagnoses or physiological monitoring [14–16]. It is not yet clear to what extent this is due to an inherent infidelity of concentration levels in the tear film to that in blood, and how much is related to the design of the sensor. It is known, however, that the tear film consists of a complex fluid environment - the lachrymal fluid has a small source at one corner of the eye from which it progresses across the ocular surface in a number of ways, mediated by blinking, gravity and fluid action, before draining into the lachrymal puncta in the opposite corner. If we can monitor the introduction, mixing and drainage of this continuous flow of lachrymal fluid, we should be in a much stronger position to draw suitably accurate conclusions regarding the concentration levels of the biomarker, and perhaps then perform measurements with sufficient fidelity to achieve a desired level of confidence in diagnostic conclusions. Sensors in existing ESCL prototypes necessarily make the gross over-simplification of treating the tear film as equivalent to a bulk homogenous fluid, and make no effort to consider a spatiotemporal concentration map of the eye. They therefore measure, most often, the concentration in some part of the lachrymal lake - an indeterminately mixed region collecting at the lower eyelid.

The development of a robust SCL technology [17,18] in recent years offers the opportunity to integrate state-of-the-art microelectrode

* Corresponding Author.

https://doi.org/10.1016/j.snb.2019.126671
Received 14 February 2019; Received in revised form 5 June 2019; Accepted 6 June 2019
Available online xxx
0925-4005/

technology into an existing platform. Using polyimide, a biocompatible polymer [19,20] with high glass transition temperature of 360 °C [21] and resistance to many chemical agents including most solvents involved in cleanroom fabrication [22], established cleanroom methods can be adapted from silicon-based fabrication to this flexible, transparent substrate. The devices made using these materials are 11 μm in thickness and can be cut into shape by a digitally controlled laser with precision on the order of tens of microns before integration into the SCL platform.

Integrating multiple microelectrodes (as opposed to macroelectrodes) in a spatial array format into the SCL platform leads to three potential advances on the existing state-of-the-art. Many different sensing sites may be

i operated in summation, creating a large signal and reducing the dependence on sensing location within the eye; or
ii operated individually to create an electrochemical still- or moving-(video) image of the tear film under the lens; or
iii each individually functionalised for a different target in order to measure multiple analytes in one device, for multimodal analysis and differential diagnoses.

Microelectrodes also have advantageous sensing properties in comparison to macroelectrodes, including increased sensitivity, faster response time and improved mass transport [23,24]; these are of particular importance when working in the tear film which is a dilute, low-volume medium [25].

We present a linear array of eight individually addressable (8 × 1) microelectrodes, using a layer stack of polyimide – gold – polyimide, closely following the fabrication process used for the SCL platform developed by Vásquez Quintero et al. [18]. While microelectrodes have previously been reported on similar substrates [26–29], they have not been designed for this purpose, and are most often intended for electrical stimulation of neurons. Moreover, in this paper we demonstrate for the first time a real-speed electrochemical 'video' of analyte distribution in an environment approaching a laminar flow regime, under a flexible device, analogous to the flow of analyte in the tear film under a SCL. Our work therefore progresses towards a spatiotemporal electrochemical system capable of tracking chemical biomarkers across the tear film, thus providing more information on the introduction, flow and drainage of these biomarkers than any existing device.

2. Materials and methods

2.1. Fabrication

A similar fabrication process to that previously described by Vásquez Quintero et al. [18] was employed in this work. This is summarised in Fig. 1 and below. A layer of polyimide (5.5 μm) was spin-coated onto a cleaned glass wafer, dried on a hot plate and cured in a nitrogen oven. An adhesion layer of Ti was sputtered (40 nm), followed by a layer of Au (60 nm). The metal layer was patterned with photolithography and wet etching. A second layer of polyimide (5.5 μm) was spin-coated to cover the gold pattern. A sputtered thin film of Al (200 nm) with adhesion layer (TiW) patterned by photolithography and wet etching functioned as a hard mask to define via holes in the top polyimide layer to expose the Au at the electrodes and the contact pads using reactive ion etching (55 min, 40 W, 150 mTorr, 15 sccm O_2, 5 sccm CHF_3). Al and TiW etchants removed the hard mask from the surface. The devices were then cut using a picosecond laser (355 nm, 12 ps, 50 kHz, 320 mW) to ablate the two layers of polyimide, and delaminated from the wafer with tweezers.

2.2. Electrochemical sensing

Ferrocenemethanol (Aldrich, 97% purity) was prepared at various concentrations in 0.1 M potassium chloride (Aldrich, 99% purity) with deionised water. Electrochemical experiments were carried out in a Faraday cage using a μAutolab potentiostat, using the on-device gold counter electrode and an external Ag/AgCl counter electrode (BASi, USA). Control and data acquisition was performed using General Purpose Electrochemical System (GPES, version 4.9).

During spatiotemporal sensing a 74HC4051 8-channel analog multiplexer was driven by a microcontroller (Arduino Nano [30], an open source hardware and software platform used to perform computation and control peripheral devices). The multiplexer was used to rapidly switch in sequence through the eight working electrodes. Data processing was carried out using algorithms written in the python programming language.

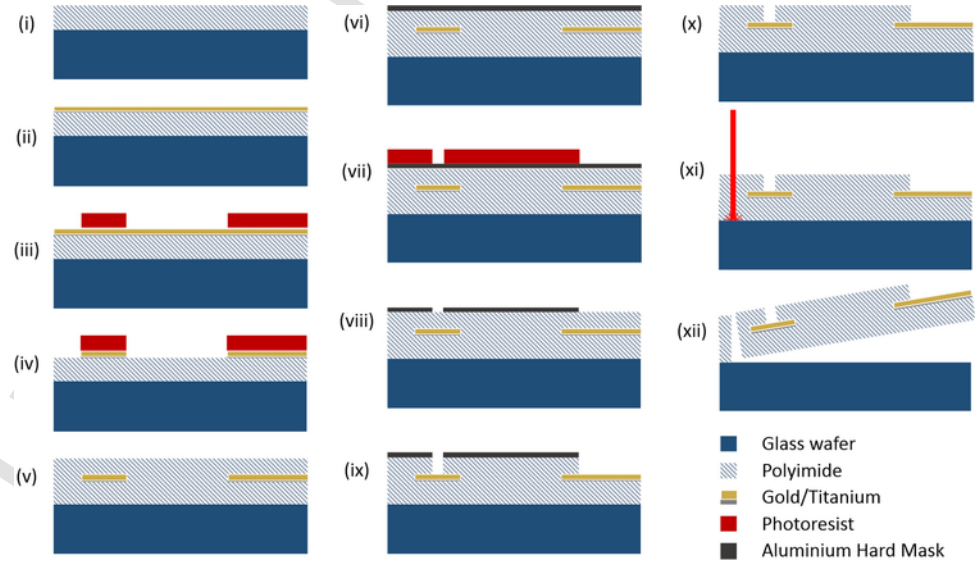

Fig. 1. Schematic cross sectional images showing the process flow at significant stages. (i) Polyimide spin-coated onto glass wafer, (ii) Au/Ti deposited, (iii) Photoresist pattern defined, (iv) Au/Ti patterned by wet etch, (v) Polyimide spin-coating, (vi) Aluminium hard mask deposited, (vii) Photoresist pattern defined, (viii) Aluminium patterned by wet etch, (ix) Polyimide etched with reactive ion etching, (x) Aluminium hard mask removed by wet etch, (xi) edge of device cut by laser, (xii) Finished device lifted off glass wafer.

3. Results and discussion

3.1. Design

The device consists of a layer of gold (60 nm thickness, with an adhesion layer of titanium, 40 nm thickness) sandwiched between two layers of polyimide, both 5.5 μm in thickness. The finished device is cut to shape using laser ablation. The total thickness of the device is 11 μm; it is flexible, and was proven to be robust during routine laboratory use. The position of the metal layer in the neutral mechanical plane protects the metal interconnects and electrode sites from damage during bending [17], while the design of the meanders [31] is optimised for incorporation into the thermoplastic polyurethane encapsulation utilised in the SCL platform [18]. A linear array of eight individually-addressable gold microelectrodes was designed to fit on one device (Fig. 2). The working electrodes are circular, 30 μm in diameter, and recessed by a depth of 5.5 μm into the device (equal to the thickness of the upper layer of polyimide). Theoretical analyses suggest that recessing the microelectrode will result in a reduction of overall analyte flux of just over 30% compared to an inlaid microdisc [32]. Each microelectrode is situated equidistant to one site of the common gold counter electrode shown on the right of Fig. 2C; an external reference electrode was used for this study.

3.2. Electrochemical characterisation

The microdisc electrodes were first characterised individually using standard cyclic voltammetry (in which current was measured during a voltage sweep from 0 V to 0.4 V to 0 V, at a scan rate of 0.1 V s^{-1}). Each showed a characteristic microelectrode response to a typical redox reporter (ferrocenemethanol, FeMeOH); an example is shown in Fig. 3.

Experimental results were analysed using the Saito equation (Eq. [1]) [33], which describes the limiting current, i_L, of a microdisc electrode in steady-state conditions:

$$i_L = 4nFDc_0r \quad (1)$$

where n is the number of electrons transferred in the reaction, F is the Faraday constant, D is the diffusion coefficient of the redox species (ferrocenemethanol), c_0 is the concentration, and r is the radius of the microdisc. We used values of $D = 10^{-10}$ m^2 s^{-1} [34] and $c_0 = 0.5$ mol m^{-3}. A mean limiting current of 1.76 nA was found, thus yielding a theoretical microdisc diameter of 182 μm – significantly higher than the observed diameter of 30 μm. This suggests some degree of surface roughness, a feature which has been found to increase the limiting current of a microdisc electrode [35]. Alternatively, a roughness factor may be estimated based on the effective area obtained by integrating the reduction peak of an H_2SO_4 cleaning cycle, and using the reported relation between charge and area (390 μC cm^{-2}) [36]. In this way, a mean roughness factor of 4.2 was obtained across the electrodes (the ratio of the effective to geometric area). This result is of the same order of magnitude to the observed increase in current (a factor of 6.1).

Surface roughness of exposed gold areas was investigated during an earlier stage of work using the same fabrication method ([18], supplementary materials) and a root-mean-square roughness of 1.75 nm was measured using this reactive ion etch power of 40 W. Scanning electron micrographs also confirmed that the gold surface of the microelectrodes exhibited a degree of surface roughness (Fig. 4). The increased current caused by this roughness is in some ways desirable, as it results in a more efficient use of the electrode area. However, the electrode performance is accordingly less well characterised, and does not agree well with the standard model for flat microdisc electrodes; this is important to note in some applications, though it was not a problem within the scope of this work.

Cyclic voltammetry was used to measure how the current responds across a range of concentration of FeMeOH, from 10 to 500 μM, and a 'blank' measurement of KCl (0.1 M). A linear current response was observed over the entire range of measurement (Fig. 5), with $R^2 > 0.999$, indicating a very high confidence in the linear fit. We took triplicate

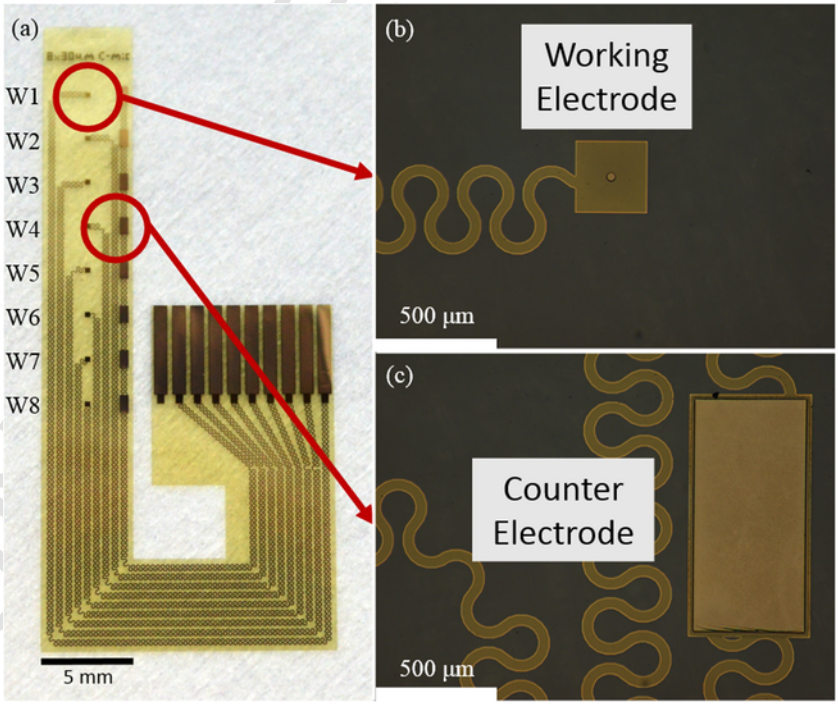

Fig. 2. (a) Photograph of the flexible microelectrode array; the positions of working electrodes W1-8 are indicated. (b) Photomicrograph of one working electrode; the 30 μm diameter disc is situated in the centre of the square. The gold serpentine connections are visible through the transparent polyimide surface. (c) Photomicrograph of one part of the counter electrode; electrical connection is shared among all counter electrode sites.

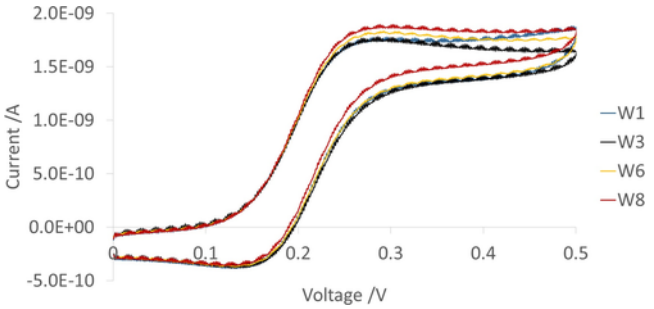

Fig. 3. Results of cyclic voltammetry performed separately on working electrodes (W1, W3, W6 and W8 shown in this figure) in ferrocenemethanol (FeMeOH, 0.5 mM) at a scan rate of 0.1 V s^{-1}.

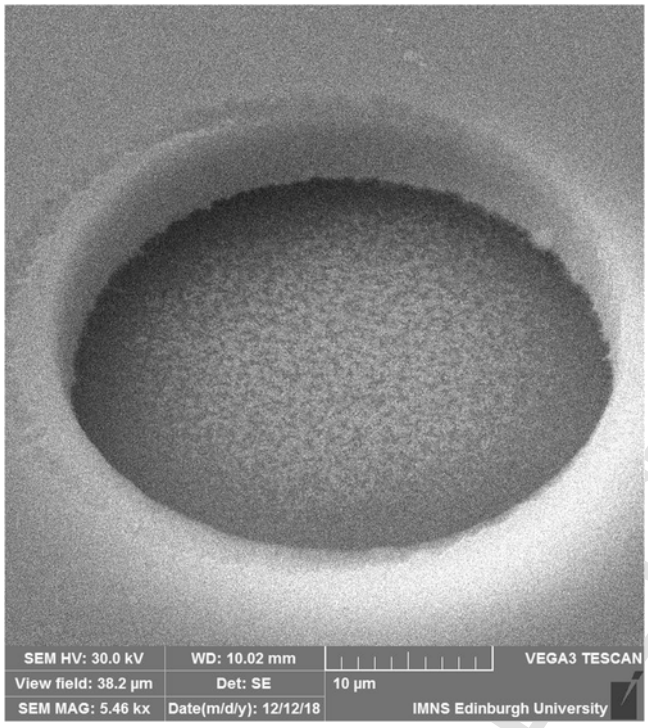

Fig. 4. Scanning electron micrograph of a microdisc electrode.

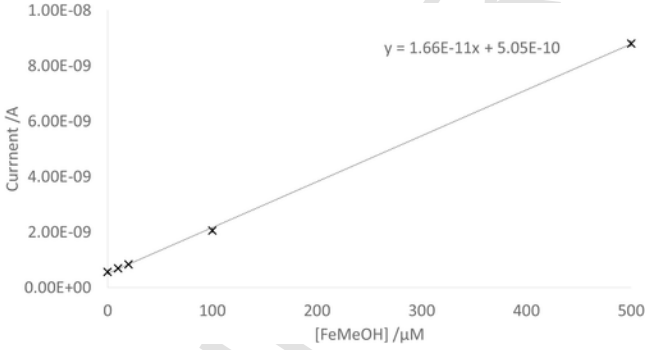

Fig. 5. Current response of a microdisc electrode to a range of concentrations of FeMeOH; error bars are included.

measurements at each concentration and used this to establish a limit of detection (LOD) following the IUPAC convention [37]:

$$x_L = \bar{x}_{bl} + k s_{bl} \quad (2)$$

where x_L is the smallest current that can be reliably detected, $\bar{x}_{bl}$ and s_{bl} are the mean and standard deviation respectively of the blank (KCl) measurement, and k is a numerical factor (we used $k = 3$ to ensure a confidence level of $> 99\%$). The LOD is obtained by substituting $x = x_L$ into the calibration function (Fig. 5), giving the lowest concentration that can be detected at our chosen confidence level. Using this method we obtained a LOD of 0.016 mM. This result is comparable to that reported by Freeman et al. [38], in which a 100 µm diameter platinum disc electrode was found to have a LOD of 0.097 mM in ferrocene carboxylic acid, a similar redox reporter. Using an area ratio as a rough guide, we can conclude that our 30 µm diameter microdisc electrodes have a LOD of the expected order of magnitude. Recessing the electrode into the polyimide substrate to a depth of 5.5 µm, which has the effect of reducing analyte flux by around 30%, may result in an elevated LOD compared to a non-recessed microdisc electrode.

3.3. Spatiotemporal sensing

Multiple-electrode sensing was carried out using an analogue multiplexer driven by a microcontroller (an Arduino Nano [30]), which addressed the electrodes one-by-one in a cyclic sequence. This switching was performed constantly at a rate of 20 Hz (20 electrodes per second) while a potentiostat was used to conduct chronoamperometric measurement at 0.4 V for 10 s. An in-device gold counter electrode was used, with an external Ag/AgCl reference electrode. Due to the rate of switching, higher currents were drawn compared to those found in cyclic voltammetry (Fig. 3), resulting from to the initial formation of the electrical double layer at the electrode site, and from parasitic capacitance, inductance and resistance in the device and the circuit beyond (see Appendix 1, Fig. A1 for schematic). Experiments were first carried out in a beaker. Calibration in KCl (0.1 M) and FeMeOH (0.5 mM) was performed, and subsequently an experiment was conducted in which FeMeOH was added by two separate injections of 1 mL volume each, using a micropipette, to a beaker of KCl (initial volume ~ 5 mL), while high-speed chronoamperometric measurements were taken as described above. Next, an on-droplet experiment was conducted to mimic a sensing environment analogous to that of a tear film under a SCL: the device was placed on top of a droplet of either KCl or FeMeOH solution to form a film of liquid between the active surface of the device and the glass underneath. After calibration, measurements were taken while FeMeOH was injected into an initial KCl droplet of volume < 1 mL. Again, FeMeOH was added by two injections of 1 mL volume, with the micropipette placed at the W7-8 (working electrodes 7-8) end of the device.

Chronoamperometric data were collected in a single data stream with no sub-categorization of the individual response of each working electrode; the raw signal effectively consisted of a repeating eight-step sequence of 50 ms chronoamperometric measurements (Fig. 6A). A range of current responses was observed between the different working electrodes (Fig. 6B). The variation in current drawn during these high-speed measurements was found to follow the variation in path length of the meandering wires in the device. The effect was corrected during calibration (see Appendix 2 for a more detailed discussion on this variation).

An algorithm was designed to detect and separate the signals from the eight individual working electrodes (W1-8). Once separated, an average current was obtained from the 25 ms to 45 ms segment of each 50 ms measurement period (chosen to avoid the initial non-Faradaic signal and any switching noise at either end of the measurement period), to generate a single data point for that time value. Linear interpolation was used to smooth the data between time points and to avoid a rolling refresh effect.

Calibration between an average 'high' value (FeMeOH, 0.5 mM) and 'zero' value (KCl, 0.1 M) was performed individually for each working electrode. Fig. 7A provides a detail of this process during the droplet experiment, showing three measurements (only W1 shown for

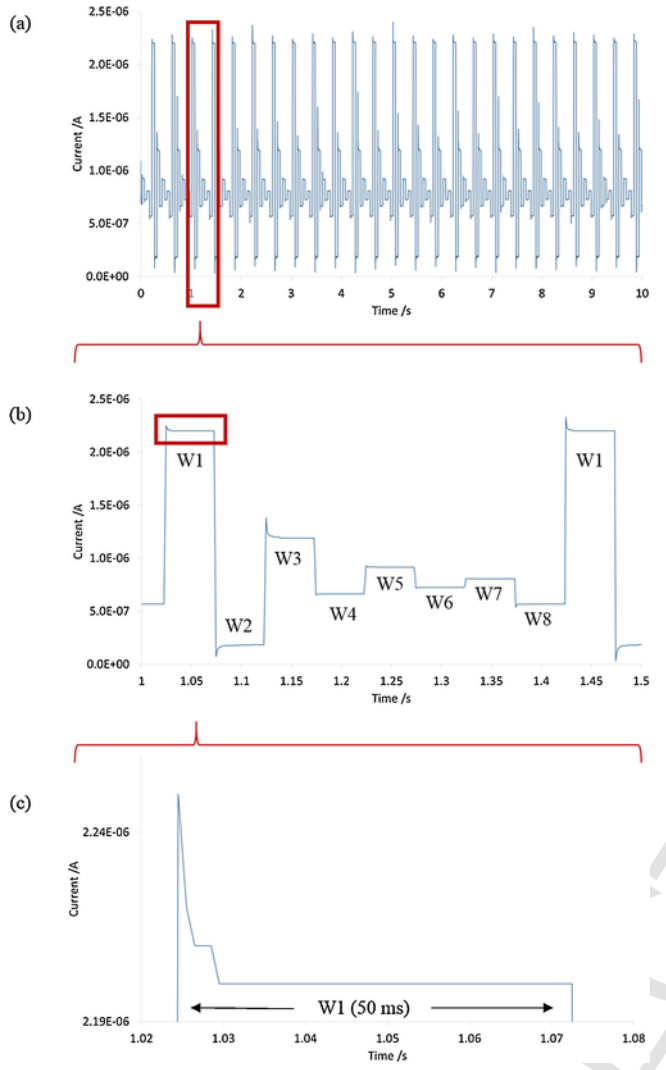

Fig. 6. (a) Current measured over a 10 s experiment in a beaker of FeMeOH (0.5 mM) with the potentiostat running a chronoamperometric program, and multiplexer performing cyclic switching through the eight working electrodes. (b) Detail highlighted in (a), showing a complete cycle of the eight electrodes (denoted W1, W2 etc). (c) Detail highlighted in (b), showing a single electrode response.

clarity): the W1 'high' (indicated with a solid horizontal line), W1 'zero' (indicated with a dotted horizontal line) and the signal generated by W1 during time-varying concentration ('KCl + FeMeOH', marked with crosses). Figs. 7B and C show the time-varying concentration at each working electrode over the 10 s measurement period for the beaker experiment and the on-droplet experiment. In the beaker experiment there was virtually no spatial inhomogeneity of concentration across the device, and thus the eight working electrodes recorded almost identical concentrations at all times. The effects of the two injections of FeMeOH can be clearly observed; the concentration rises slowly as the FeMeOH mixes with the KCl solution.

In the on-droplet experiment, the measured concentration rises very quickly upon the first injection. This is likely due to bulk flow of FeMeOH pushing the initial KCl film away. Diffusive and turbulent mixing would have taken place at the interface of the two fluids, but in the laminar flow regime it is likely that the incoming fluid simply pushed away the majority of the initial fluid with only a minor amount of mixing. Thus, the concentration rises to nearly 0.5 mM after the first injection (I1). The effect of the second injection (I2) is not so pronounced, because the concentration under the electrodes was already fairly high. It is also possible to observe at various times a difference in the concentrations observed at each electrode (Fig. 7C, e.g. at the second injection, t = 8), as fluid mixing was less efficient in this experiment compared to the beaker experiment, resulting in a not-always-homogeneous concentration across the device. These effects are explored in more detail with reference to Figs. 8A, B, but in Fig. 7C it is already clear that W1-2 experienced a slightly lower concentration throughout the experiment; since FeMeOH was injected from the W7-8 end of the device, it is likely that the initial KCl droplet was pushed in the direction of W1-2, resulting in this lower concentration. Fig. 8C also shows that the W1-2 end of the device was situated closer to the glass at the start of this experiment, such that the KCl situated there would have moved and mixed less readily than the rest of the droplet.

In order to better visualise the concentration flow the data were rescaled between 0 and 1, which was then used to prepare a colour map representing concentration at each electrode site (Fig. 8B). This can be viewed in real time (Supplementary Materials OR Fig. 8D), while Fig. 8B shows some representative frames from the video. It is possible to see in these frames the initial injection of FeMeOH (from the W7-8 end of the device, e.g. t = 2.59–2.84) followed by mixing and homogenisation after I1 (e.g. t = 3.14). The effects of I2 can be seen in the same way (e.g. t = 8.39, where a larger volume underneath W3-8 perhaps allowed circular mixing which was observed at W3-4 before W5-6) and the unmixed solution at W1-2 (e.g. t = 9.54). When viewed in its entirety, the electrochemical 'video' provides a clearer visualisation of the flow of analyte across the device, with both bulk flow and diffusive mixing visible.

4. Conclusions

In this work, we have shown an electrochemical 'video' illustrating concentration varying at real-speed under a flexible multi-electrode device, leading the way towards a new class of intelligent sensing systems.

In standard electrochemical characterisation procedures the device showed expected behaviour from a microdisc electrode in cyclic voltammetry. Based on the oxidation of ferrocenemethanol, these microelectrodes generated a 610% higher current than that theoretically predicted, which we attributed to roughness of the gold electrodes as supported by that found in scanning electron micrographs. We calculated a LOD of 0.016 mM, which is within the expected order of magnitude for this class of electrode.

In order to perform spatiotemporal measurements, data were captured using chronoamperometry while cycling through the eight electrodes at a rate of 20 Hz. After calibration and signal processing, we were able to produce an electrochemical 'video' of local concentration across the device, showing the effect of two injections of FeMeOH into KCl solution and the subsequent mixing and homogenisation of the fluid, first in a beaker and then in a droplet situated between the device and a glass surface. The characteristics of fluid effects in these two environments were observed in the electrochemical 'video'.

The ability to create a spatiotemporal concentration map of the tear film will pave the way to a deeper understanding of how the lachrymal fluid flows across the cornea whilst wearing a contact lens. This is central to the understanding of various contact lens-related conditions, such as contact lens induced dry-eye [39]. It may also help us to monitor the introduction, mixing and drainage of lachrymal fluid in the eye, leading to a better understanding of the measurements made in ESCLs, and ultimately to improve confidence in the diagnoses and conclusions from physiological monitoring using ESCLs. In addition, it could be used to help quantify drug uptake during ocular drug delivery.

The demonstration of this system on a device made using state-of-the-art fabrication methods developed for an existing SCL platform [18] builds on established work with a route towards clinical use. The system introduces very little additional complexity compared to exist-

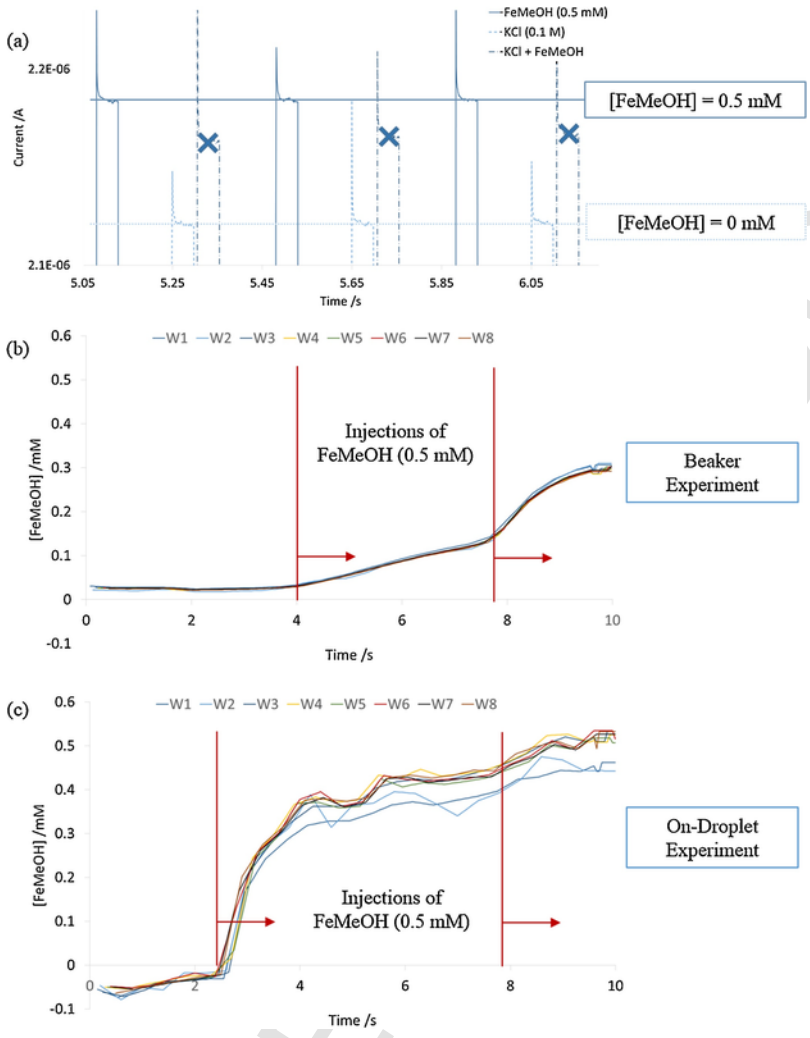

Fig. 7. (a) Detail of the signal from W1 during on-droplet measurements of 'high' (FeMeOH 0.5 mM), 'zero' (KCl 0.1 M) and variable ('KCl + FeMeOH', where FeMeOH was injected into a KCl droplet at the W7-8 end of the device) concentrations. Annotations illustrate the calibration method. (b) FeMeOH concentration at all electrodes throughout the 10 s beaker experiment. Injections of FeMeOH are illustrated. (c) FeMeOH concentration at all electrodes throughout the 10 s on-droplet experiment. Injections of FeMeOH are illustrated. (Note: a single anomalous data point has been removed in W1).

ing electrochemical systems which have been successfully miniaturised for SCL platforms [3]. The primary addition is an analogue multiplexer working in an automatic, continuous mode, a function which requires a relatively small amount of circuitry, and which avoids the need for multiple potentiostats.

We envisage that our future work will apply these results to an established SCL platform and progress closer to performing spatiotemporal electrochemistry in an ocular environment. In order to increase current and therefore improve sensitivity, islands of connected arrays of microdisc electrodes may be used instead [34]. This sensing technique may have additional applications: for example, using the existing linear array in fluid monitoring for microfluidics and lab-on-a-chip systems, and, when extended into a two-dimensional array, developing surface concentration maps in smart tattoo-based sensing, smart wound dressings, other medical applications, and even further afield.

CRediT authorship contribution statement

Matthew Donora: Conceptualization, Data curation, Formal analysis, Funding acquisition, Investigation, Methodology, Project administration, Software, Validation, Visualization, Writing - original draft, Writing - review & editing. **Eva Gonzalez-Fernandez:** Methodology, Validation, Writing - review & editing. **Andrés Vásquez Quintero:** Methodology, Project administration, Validation, Writing - review & editing. **Herbert De Smet:** Funding acquisition, Project administration, Resources, Supervision, Writing - review & editing. **Ian Underwood:** Funding acquisition, Project administration, Resources, Supervision, Writing - review & editing.

Acknowledgements

This work was supported by the EPSRC CDT in Integrative Sensing and Measurement, Grant Number EP/L016753/1 in the form of a studentship and additional travel allowance to support the collaborative activity with University of Ghent, and by the EPSRC-funded Implantable Microsystems for Personalised Anti-Cancer Therapy (IMPACT) programme, Grant NumberEP/K034510/1. The authors would also like to thank Ilka Schmueser, Paul Sullivan and Yuchen Shang for their help in this work.

Appendix A.

Appendix B.

In electrochemical characterisation using cyclic voltammetry, at a sweep rate of 0.1 V s^{-1}, the current responses of the electrodes was found to be very similar (Fig. 3). However, in high-speed chronoamperometric measurements (voltage step occurs at a rate greater than 400 V

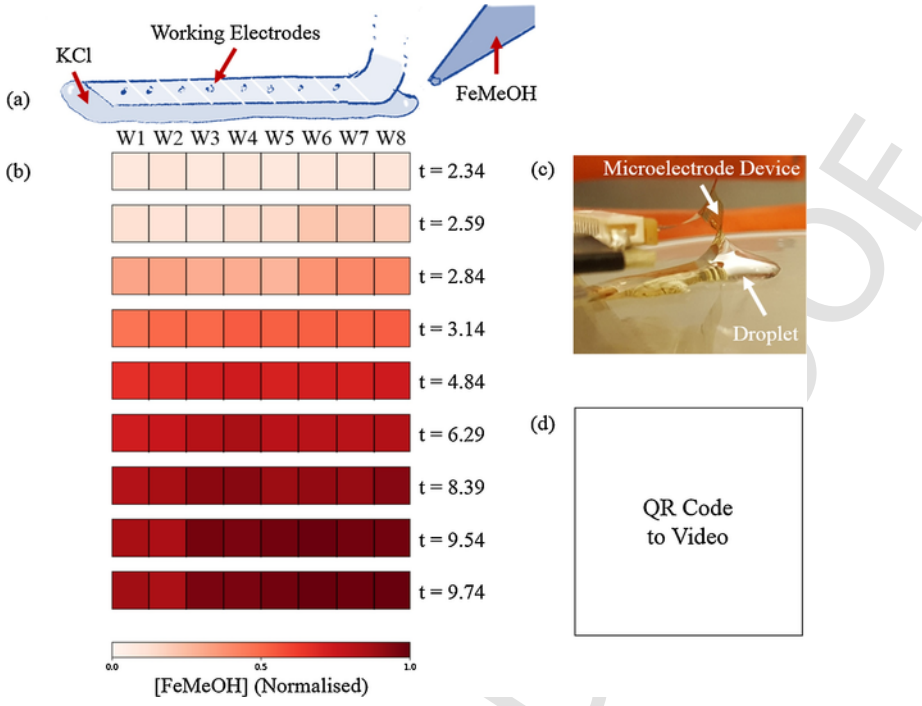

Fig. 8. (a) Illustration of the droplet experiment in schematic cross-section. FeMeOH is injected into a droplet of KCl from the W8 end of the microelectrode device (reference electrode not shown). (b) Still frames from the colour map video of concentration across the device. Time points are chosen to illustrate various features of the flow, particularly at I1 ($t \approx 2.5$) and I2 ($t \approx 8$). See Supplementary Materials for full video. (c) Photograph of experimental setup, showing the microelectrode device resting on a KCl droplet (reference electrode not shown). (d) QR Code to full electrochemical 'video'.

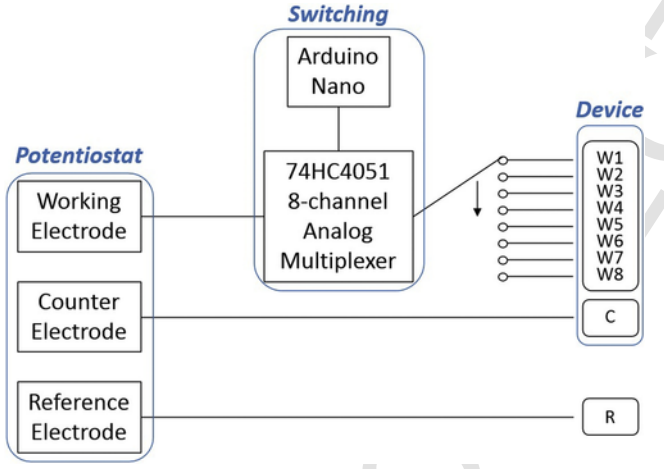

Fig. A1. Schematic of the circuitry used for spatiotemporal experiments, illustrating the connections of the potentiostat (μAutolab) to the working electrodes (W1-8), via an analogue multiplexer driven by a microcontroller (Arduino Nano); to the on-device counter electrode (C); and to the external reference electrode (R).

s^{-1}), a range of current responses was observed between electrodes (Fig. 6B). In high-speed measurements, the effects of parasitic capacitance, inductance and resistance are of far greater importance. The current derived from the electrochemical response is combined with contributions from these additional effects. In our study, the variation in current response between the working electrodes was found to follow the variation in path length of meandering connections within the device (Fig. B1; path length of in-device connections is variable, see Fig. 2A). It follows that part of the variation in current drawn during high-speed measurement derives from the variation in length of electrical connections in the device. Wire connections in the subsequent circuitry were also not always equal between electrodes; therefore it is likely that similar effects contributed beyond the device as well as within.

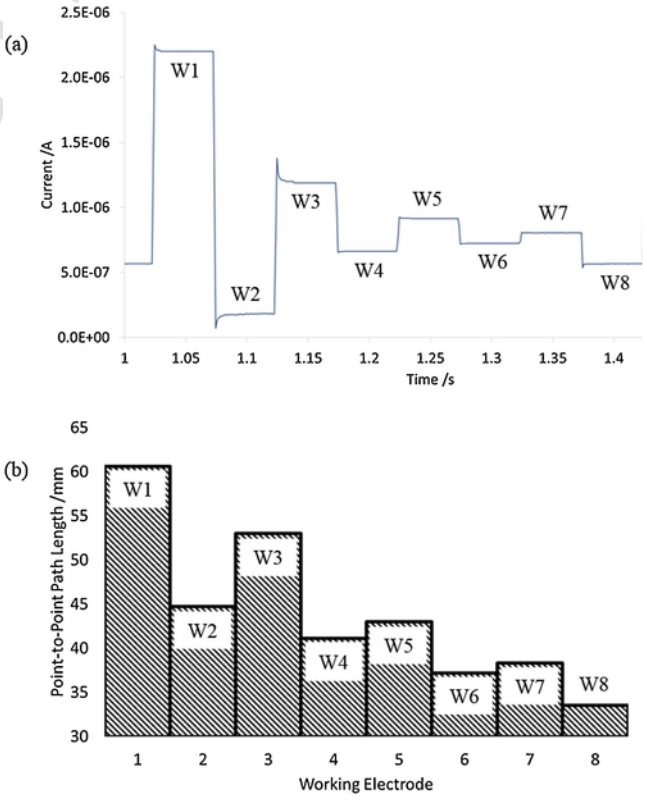

Fig. B1. (a) Current measured during high-speed chronoamperometry, with the response of each working electrode illustrated (duplicated from Fig. 6B); (b) Electrical path length of each working electrode as measured from electrode to connection pad in-device. Point-to-point path length is illustrated here; the true path length following the meanders would be a multiple of these values).

Electrical path length is greatly increased using meander connections rather than straight wires. In a small device, proximity of connection paths is also usually increased with meanders. It has been shown that meandering connections can improve mechanical stability of electrical connections travelling in the radial direction in a moulded smart contact lens, but they are not necessary in the circumferential direction [18]. Although in this study the effect of parasitic capacitance, induction and resistance was easily corrected for during calibration, it is worth noting this result of using meandering connections and potentially limiting their use when not necessary, e.g. for wires in the circumferential direction of a smart contact lens.

Appendix C. Supplementary data

Supplementary material related to this article can be found, in the online version, at doi:https://doi.org/10.1016/j.snb.2019.126671.

References

[1] H. Yao, A.J. Shum, M. Cowan, I. Lähdesmäki, B.A. Parviz, A contact lens with embedded sensor for monitoring tear glucose level, Biosens. Bioelectron. 26 (7) (2011) 3290–3296.

[2] N. Thomas, I. Lähdesmäki, B.A. Parviz, A contact lens with an integrated lactate sensor, Sens. Actuators, B Chem. 162 (1) (2012) 128–134.

[3] H. Yao, et al., A contact lens with integrated telecommunication circuit and sensors for wireless and continuous tear glucose monitoring, J. Micromech. Microeng. 22 (July (7)) (2012) 075007.

[4] A.J. Bandodkar, J. Wang, Non-invasive wearable electrochemical sensors: a review, Trends Biotechnol. 32 (7) (2014) 363–371.

[5] Y.-T. Liao, H. Yao, A. Lingley, B. Parviz, B.P. Otis, A 3-uW CMOS glucose sensor for wireless contact-lens tear glucose monitoring, IEEE J. SolidState Circuits 47 (January (1)) (2012) 335–344.

[6] Y.J. Kim, J. Maeng, P.P. Irazoqui, Eyeglasses-powered, contact lens-like platform with high power transfer efficiency, Biomed. Microdevices 17 (4) (2015) 1–9.

[7] J. Pandey, Y.-T. Liao, A. Lingley, R. Mirjalili, B. Parviz, B.P. Otis, A fully integrated RF-Powered contact Lens With a single element display, IEEE Trans. Biomed. Circuits Syst. 4 (December (6)) (2010) 454–461.

[8] J.-C. Chiou, S.-H. Hsu, Y.-C. Huang, G.-T. Yeh, W.-T. Liou, C.-K. Kuei, A wirelessly powered smart contact Lens with reconfigurable wide range and tunable sensitivity sensor readout circuitry, Sensors 17 (1) (2017) 108.

[9] K. Mansouri, T. Shaarawy, Continuous intraocular pressure monitoring with a wireless ocular telemetry sensor: initial clinical experience in patients with open angle glaucoma, Br. J. Ophthalmol. 95 (5) (2011) 627–629.

[10] Sensimed, 2015, [Online]. Available: http://www.sensimed.ch/en/.

[11] J. Park, et al., Soft, smart contact lenses with integrations of wireless circuits, glucose sensors, and displays, Sci. Adv. 4 (January (1)) (2018), eaap9841.

[12] J. Kim, et al., Wearable smart sensor systems integrated on soft contact lenses for wireless ocular diagnostics, Nat. Commun. 8 (2017).

[13] J. De Smet, A. Avci, R. Beernaert, D. Cuypers, H. De Smet, Design and wrinkling behavior of a contact lens with an integrated liquid crystal light modulator, IEEE/OSA J. Disp. Technol. 8 (5) (2012) 299–305.

[14] J.T. Baca, D.N. Finegold, S.A. Asher, Tear glucose analysis for the noninvasive detection and monitoring of diabetes mellitus, Ocul. Surf. 5 (October (4)) (2007) 280–293.

[15] J.T. Baca, C.R. Taormina, E. Feingold, D.N. Finegold, J.J. Grabowski, S.A. Asher, Mass spectral determination of fasting tear glucose concentrations in nondiabetic volunteers, Clin. Chem. 53 (7) (2007) 1370–1372.

[16] B. Peng, J. Lu, A.S. Balijepalli, T.C. Major, B.E. Cohan, M.E. Meyerhoff, Evaluation of enzyme-based tear glucose electrochemical sensors over a wide range of blood glucose concentrations, Biosens. Bioelectron. 49 (2013) 204–209.

[17] A.V. Quintero, D. Briand, N.F. De Rooij, Flip-chip integration of Si bare dies on polymeric substrates at low temperature using ICA vias made in dry film photoresist, J. Micromech. Microeng. 25 (4) (2015).

[18] A. Vásquez Quintero, R. Verplancke, H. De Smet, J. Vanfleteren, Stretchable electronic platform for Soft and smart contact Lens applications, Int. J. Adv. Mater. Technol. 2 (August (8)) (2017) 1700073.

[19] R.R. Richardson, J.A. Miller, W.M. Reichert, Polyimides as biomaterials: preliminary biocompatibility testing, Biomaterials 14 (January (8)) (1993) 627–635.

[20] P. Starr, C.M. Agrawal, S. Bailey, Biocompatibility of common polyimides with human endothelial cells for a cardiovascular microsensor, J. Biomed. Mater. Res. A 104 (February (2)) (2016) 406–412.

[21] HD MicroSystems, PI-2600 Series – Low Stress Applications, [Online]. Available: https://www.dupont.com/content/dam/dupont/products-and-services/electronic-and-electrical-materials/semiconductor-fabrication-and-packaging-materials/documents/PI-2600_ProcessGuide.pdf, 2009.

[22] A. Georgiev, D. Dimov, E. Spassova, J. Assa, P. Dineff, G. Danev, Chemical and physical properties of polyimides: biomedical and engineering applications, in high performance polymers - polyimides based - from chemistry to applications, InTech (2012).

[23] I. Schmueser, A.J. Walton, J.G. Terry, H.L. Woodvine, N.J. Freeman, A.R. Mount, A systematic study of the influence of nanoelectrode dimensions on electrode performance and the implications for electroanalysis and sensing, Faraday Discuss. 164 (2013) 295.

[24] R.M. Wightman, Voltammetry with microscopic electrodes in new domains, Science 240 (April (4851)) (1988) 415–420.

[25] U. Stahl, M. Willcox, F. Stapleton, Osmolality and tear film dynamics, Clin. Exp. Optom. 95 (January (1)) (2012) 3–11.

[26] S.R.I. Gabran, et al., 3-d flexible nano-textured high-density microelectrode arrays for high-performance neuro-monitoring and neuro-stimulation, IEEE Trans. Neural Syst. Rehabil. Eng. 22 (September (5)) (2014) 1072–1082.

[27] F. Waschkowski, et al., Development of very large electrode arrays for epiretinal stimulation (VLARS), Biomed. Eng. Online 13 (1) (2014) 11.

[28] T. Li, B. Sun, K. Xia, Q. Zeng, T. Wu, M.S. Humayun, Design and fabrication of a high-density flexible microelectrode array, 2017 IEEE 12th International Conference on Nano/Micro Engineered and Molecular Systems (NEMS), 2017299–302.

[29] M.L. Khraiche, W.B. Phillips, N. Jackson, J. Muthuswamy, Sustained elevation of activity of developing neurons grown on polyimide microelectrode arrays (MEA) in response to ultrasound exposure, Microsyst. Technol. 23 (August (8)) (2017) 3671–3683.

[30] Arduino Nano Guide [Online]. Available: https://www.arduino.cc/en/Guide/ArduinoNano.

[31] R. Verplancke, F. Bossuyt, D. Cuypers, J. Vanfleteren, Thin-film stretchable electronics technology based on meandering interconnections: fabrication and mechanical performance, J. Micromech. Microeng. 22 (1) (2012).

[32] P.N. Bartlett, S.L. Taylor, An accurate microdisc simulation model for recessed microdisc electrodes, J. Electroanal. Chem. 453 (1–2) (1998) 49–60.

[33] Y. Saito, A theoretical study on the diffusion current at the stationary electrodes of circular and narrow band types, Rev. Polarogr. 15 (6) (1968) 177–187.

[34] I. Schmüser, The Design, Fabrication and Characterisation of Nanoelectrodes for Electrochemical Sensing, 2015.

[35] K.G. Shah, V.M. Tolosa, A.C. Tooker, S.H. Felix, S.S. Pannu, Improved chronic neural stimulation using high surface area platinum electrodes, Conf. Proc. IEEE Eng. Med. Biol. Soc. 2013 (2013) 1546–1549.

[36] S. Trasatti, O.A. Petrii, Real surface area measurements in electrochemistry, J. Electroanal. Chem. 327 (June (1–2)) (1992) 353–376.

[37] A.D. McNaught, A. Wilkinson, IUPAC, Compendium of Chemical Terminology, 2nd edition, Blackwell Scientific Publications, 1997.

[38] N.J. Freeman, et al., Comparison of the performance of an array of nanoband electrodes with a macro electrode with similar overall area, Phys. Chem. Chem. Phys. 15 (21) (2013) 8112.

[39] L.C. Thai, A. Tomlinson, M.G. Doane, Effect of contact lens materials on tear physiology, Optom. Vis. Sci. 81 (3) (2004) 194–204.

Matthew Donora received his degree in Physics from the University of Oxford in 2014, specialising in quantum information processing, condensed matter and laser physics. He obtained a distinction in the MSci Biomedical Engineering from Imperial College London in 2015, with a project on design, synthesis and characterisation of polyaniline nanoparticles for photothermal cancer therapy. He is pursuing his PhD in electrochemical sensors for smart contact lenses at the University of Edinburgh.

Eva Gonzalez-Fernandez received her degree in Chemistry in 2007 from the University of Oviedo (Spain) and gained her PhD from the same university in 2012, working on the development of electrochemical nucleic acid-based biosensors. After a period in industry, in January 2014 she joined Prof. Bradley's lab in the University of Edinburgh as a Postdoctoral Researcher, where she was involved in the IMPACT project (EPSRC-funded) working on development of electrochemical biosensors for implantable microsystems for personalised anti-cancer therapy. She recently joined a start-up company as a scientist, where she develops electrochemical-based platforms for bioanalysis.

Andrés Vásquez Quintero obtained his Ph.D. at Ecole Polytechnique Fédérale de Lausanne (EPFL), (Switzerland) in 2015, in topics related to Microsystems/MEMS, Smart electronics packaging, flexible sensing devices and ultra-thin hybrid flexible integration. He is a former postdoc fellow funded by the SNSF (Swiss National Science Foundation) and the Marie Skłodowska Curie IntraEuropean (MSCA-Horizon 2020) grants. His work involves the study of novel smart packaging solutions for medical devices, either implantable or wearable. From 2016 on he works for IMEC (Belgium), as a Specialist Researcher. From September 2018, he was appointed as part time Assistant Professor at the University of Ghent.

Herbert De Smet received his PhD degree from Ghent University in 1994. He is presently a Full Professor at the same university in the do-

main of 'Integrated intelligent sensors and metrology'. He has (co-)authored more than 200 publications and supervised 11 PhDs. His present research is focused on the design and technology of microsystems that can be integrated into e.g. smart contact lenses.

Ian Underwood is Head of the Institute for Integrated Micro and Nano Systems and Professor of Electronic Displays at the University of Edinburgh. He was awarded a PhD in Applied Optics there in 1987. He has been a Fulbright Scholar and is a Fellow of the Royal Academy of Engineering and the Royal Society of Edinburgh.